Build Simul (2020) 13: 887–896
https://doi.org/10.1007/s12273-020-0623-4

A numerical study of ventilation strategies for infection risk mitigation in general inpatient wards

Manoj Kumar Satheesan, Kwok Wai Mui, Ling Tim Wong (✉)

Department of Building Services Engineering, The Hong Kong Polytechnic University, Hong Kong, China

Abstract

Aerial dispersion of human exhaled microbial contaminants and subsequent contamination of surfaces is a potential route for infection transmission in hospitals. Most general hospital wards have ventilation systems that drive air and thus contaminants from the patient areas towards the corridors. This study investigates the transport mechanism and deposition patterns of Middle East Respiratory Syndrome Coronavirus (MERS-CoV) within a typical six bedded general inpatient ward cubicle through numerical simulation. It demonstrates that both air change and exhaust airflow rates have significant effects on not only the airflow but also the particle distribution within a mechanically ventilated space. Moreover, the location of an infected patient within the ward cubicle is crucial in determining the extent of infection risk to other ward occupants. Hence, it is recommended to provide exhaust grilles in close proximity to a patient, preferably above each patient's bed. To achieve infection prevention and control, high exhaust airflow rate is also suggested. Regardless of the ventilation design, all patients and any surfaces within a ward cubicle should be regularly and thoroughly cleaned and disinfected to remove microbial contamination. The outcome of this study can serve as a source of reference for hospital management to better ventilation design strategies for mitigating the risk of infection.

Keywords

ventilation,
bioaerosol dispersion,
indoor air quality (IAQ),
infection risk,
hospital general ward,
computational fluid dynamics (CFD)

Article History

Received: 26 November 2019
Revised: 16 January 2020
Accepted: 15 February 2020

1 Introduction

Hospitals are designed to accommodate a large number of patients with varying degrees of disease severity. As inpatient care facilities such as general medical and surgical hospitals are used by patients, healthcare workers and visitors simultaneously, the susceptibility of these people to hospital-acquired infections (HAIs) or nosocomial infections is reasonably high (Giannini et al. 2009). The largest nosocomial outbreak of Severe Acute Respiratory Syndrome (SARS) in Hong Kong, China and the recent outbreak of Middle East Respiratory Syndrome (MERS) in South Korean hospitals have had substantial morbidity and mortality (Oh et al. 2018; Tang et al. 2015). The three widely known transmission routes of SARS coronavirus (SARS-CoV) and influenza viruses are close contact, long-range airborne and fomite (Xiao et al. 2018). Although close contact is generally regarded as the possible transmission route of MERS coronavirus (MERS-CoV) (Zumla et al. 2015), studies have indicated that airborne and fomite are other possible modes of MERS-CoV transmission (Kim et al. 2016; Van Doremalen et al. 2013). There is also sufficient evidence to support that an association exists between ventilation strategies and dissemination of nosocomial pathogens in indoor environments (Li et al. 2007). Hence, it is essential to revise and update current ventilation design strategies to contain potential outbreaks caused by novel emerging viruses in the future.

Infections are explicitly considered in the ventilation requirements for healthcare facilities (Li et al. 2015). Most general hospital wards have ventilation systems that drive air from the patient areas to the circulation areas. Airborne pathogens can thus spread from a ward cubicle to the rest of the ward and lead to a potential for nosocomial outbreaks. Although it is widely assumed that increasing the air change rate (ACH) can reduce infection risks, it was shown that the risk of exposure to pathogens could increase with an increased ventilation rate under certain circumstances

E-mail: beltw@polyu.edu.hk

(Bolashikov et al. 2012; Pantelic and Tham 2013). Several studies have also emphasized that apart from ACH, the design of a ventilation system is a determinant controlling contaminant flow paths (Ghia et al. 2012; Licina et al. 2015; Memarzadeh and Xu 2012; Pantelic and Tham 2013). As there is a paucity of guidelines or strategies for general ward ventilation (Beggs et al. 2008; Chaudhury et al. 2005; Roy and Milton 2004), a review of present nosocomial infection control practices for presumably low risk zones and unprotected areas such as a general ward is all-important (Humphreys 2006; Wan et al. 2007).

To get meaningful estimations of the transport and deposition of pathogens in a mechanically ventilated space, accurate prediction of airflow pattern is essential. With the advent of improved turbulence modelling and computing power, the application of computational fluid dynamics (CFD) to indoor environment simulation has been on an increasing trend (Nielsen 2015). Under varied operating conditions in an indoor environment with high temporal and spatial resolution, CFD numerical simulation techniques provide insights into the overall airflow and bioaerosol distribution (Chao et al. 2008; Zhang and Chen 2007). In fact, CFD techniques have been used to estimate ventilation effectiveness for contaminant removal in healthcare facilities. As the number of research studies on ventilation systems for general inpatient wards with respect to air change rate and exhaust airflow rate is limited, this study evaluates the combined impacts of these two parameters on the airflow as well as infection risk distributions of droplet nuclei of size 0.167 μm (i.e. MERS-CoV) within an air-conditioned general inpatient ward cubicle. Moreover, a simple yet cost-effective ventilation system design that can minimize the risk of infection in an existing hospital ward is proposed.

2 Methodology

2.1 Infection transmission within a general inpatient ward

The risk of infection increases with increasing pathogen exposure. Even a single pathogen can initiate the onset of an infectious disease in a susceptible person (Nicas et al. 2004; Wells 1955). Based on the bioaerosol transport and deposition mechanism, this study classified the types of infection transmission in a general inpatient ward environment into two categories: (1) cross infection within a ward cubicle; and (2) infection from a ward cubicle to the corridor.

2.1.1 Cross infection within a ward cubicle

The deposition of particles in patients due to the exhalation of pathogens by other patients accommodated in the same ward can lead to cross infection. The severity of cross infection among patients depends on the location of each patient and the overall airflow distribution pattern within the ward environment. Exposure to infection due to the inhalation or deposition of particles expelled by other patients through sneezing (Infectors) can be estimated for a patient i (Receptor Exposure):

$$E_i = \sum_{j=1}^{n} e_j; \quad j \neq i \tag{1}$$

where E_i is the fractional exposure count for patient i, e_j is the fractional emission from patient j and n is the total number of patients. Based on this expression, the locations with the maximum and minimum risks of cross infection can be determined for the patients within the same ward cubicle.

General inpatient wards in hospitals are recommended to have a relative humidity between 30% and 60% (ASHRAE 2013a). As MERS-CoV can survive for up to 72 hours on plastic or steel surfaces at a room temperature of 20 °C and a humidity of 40% (Oh et al. 2018) and a portion of the exhaled particles will deposit to surfaces such as the ceiling, floor and walls in the ward, this study also took infection through surface contamination into account. Based on the three deposition ratios expressed in Eq. (2), namely wall deposition ratio r_w, ceiling deposition ratio r_c and floor deposition ratio r_f, the infection transmission through surface contamination under all ventilation scenarios considered in this study can be estimated.

$$r_w = \frac{\sum_{i=1}^{n} n_{w_i}}{n \cdot n_s}; \quad r_c = \frac{\sum_{i=1}^{n} n_{c_i}}{n \cdot n_s}; \quad r_f = \frac{\sum_{i=1}^{n} n_{f_i}}{n \cdot n_s} \tag{2}$$

where n_s is the number of particles expelled by an individual patient through sneezing, and n_w, n_c and n_f are the numbers of particles from the sneezing deposited onto the walls, ceiling and floor respectively.

2.1.2 Infection from a ward cubicle to the corridor

The dispersion of particles that were expelled by sneezing from an infected patient in a ward cubicle to the corridor was taken as the infection from a ward cubicle to the corridor. It was noted that these particles could also spread to adjacent ward spaces connected to the corridor (Chen et al. 2011). The number of particles being exhausted to the corridor n_e can be estimated based on the exhalation rates of individual supine patients in their respective beds. Using the exhausted ratio r_e for individual patients as expressed in Eq. (3), locations of the patients who contribute the most and the least to the spread of infection to the corridor can be determined.

$$r_e = \frac{n_e}{n_s} \quad (3)$$

2.2 Ventilation scenarios

A typical semi enclosed six bedded general inpatient ward cubicle with dimensions 7.5 m (L) × 6 m (W) × 2.7 m (H) and a between-bed spacing of 1 m as illustrated in Fig. 1 was used in this study (Li et al. 2005; Yu et al. 2017). The cubicle was mechanically ventilated (with a positive pressure towards the corridor) and accommodated six supine patients. The supply air, i.e. mixed air estimated based on the room volume and air change rates (3 h^{-1}–13 h^{-1}), was delivered to the cubicle through four ceiling mounted diffusers. In the base case as shown in Fig. 1(a), the supply air and ward air exhausted to the corridor were set to be equal for all air change rates. For exhausting 10% and 50% of supply air (i.e. EA = 10% and EA = 50%), local exhaust grilles (grille size 0.5 m × 0.2 m) were installed as depicted in Fig. 1(b). After the extraction by exhaust grilles, the rest of the cubicle air was exhausted towards the corridor.

2.3 Numerical simulation

2.3.1 *Airflow field and grid modelling*

The airflow distribution and the transport mechanisms of bioaerosols in the ward cubicle were investigated using a finite volume based CFD code (Ansys Fluent 13.0). The numerical simulation model consists of a continuum phase (air) and a discrete phase (droplet nuclei). In this study, the governing equations of continuity, momentum and energy for the continuum phase were based on an Eulerian framework, and the discrete phase was modelled by a Lagrangian framework (Wong et al. 2010). The three-dimensional airflow was modelled as a steady-state incompressible turbulent flow. CFD possess miscellaneous number of turbulence models, although it is very difficult to pinpoint one turbulence model that outperforms others for all class of problems. Hence, the turbulence model selection is a compromise based on factors such as flow physics involved, established practice for predicting a particular set of problem, computational resources, accuracy level and simulation time (Gao and Niu 2005). Numerous studies on turbulent indoor airflow have been carried out through Reynolds-averaged Navier Stokes (RANS) simulations, whereas for some case studies large eddy scale simulations (LES) have been preferred to provide accurate prediction of flow field variables. However, LES demands much higher grid requirements as well as computational time compared to RANS, which makes RANS widely used (Blocken 2018). The Reynolds-averaged Navier Stokes (RANS) equation greatly reduces the complexity involved in the simulation of turbulent flows. The equations have time averaged flow field variables which would eliminate the turbulent fluctuations. Although, this simplification leads to the creation of additional Reynolds stress tensors which are unknowns within the equation and leads to closure issues. The Eddy viscosity turbulence modelling provides closure to equations and the most preferred eddy viscosity turbulence model to simulate the indoor airflow distribution is the renormalization group (RNG) k-ε. The RNG k-ε model, was chosen to model the air turbulence in this study, as it offers better accuracy, stability and computing efficiency for low reynolds number as well as near wall flows (Chen 1995; Zhang and Chen 2006; Zhang et al. 2007). The diffuser inlets were defined as velocity-inlet, while corridor and exhaust grilles were treated as outflow boundary condition. Ansys Fluent treats outflow boundaries as having zero diffusion flux for all flow variables as well as it incorporates an overall mass balance correction. Furthermore, outflow with flow rate weighting option enables the user to have multiple outflow boundaries with fractional flow rate through each boundary (ANSYS 2010). A second-order upwind scheme was applied to discretize the governing equations while the SIMPLE algorithm was used for the pressure-velocity coupling in the continuum phase. The metabolic rate of a reclining patient was assumed to be 0.8 MET

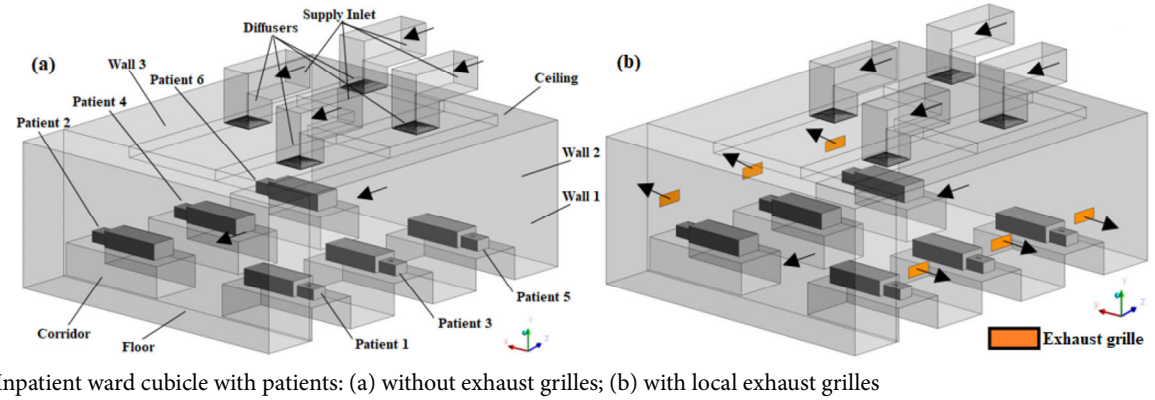

Fig. 1 Inpatient ward cubicle with patients: (a) without exhaust grilles; (b) with local exhaust grilles

(ASHRAE 2013b) and half of the heat (23.3 W·m^{-2}) from each patient is assumed to be transferred through convection (Qian and Li 2010; Hang et al. 2014). A constant heat flux thermal boundary condition was uniformly imposed on the whole surfaces of the supine patients (Shen et al. 2013). Apart from walls of heat sources (patients), all other walls were treated as adiabatic. Smooth no-slip condition is applied at all walls. In order to reduce modelling complexity arising from density differences due to temperature gradients, the Boussinesq approximation was employed (Zeytounian 2003).

The computational domain of inpatient ward was split in to multiple fluid zones. ICEM-CFD 13.0 was utilized to generate hexahedral mesh for these individual computational cell zones. The individual mesh files are then merged together using the tmerge filter functionality. In tmerge, before the individual meshes are combined together to one mesh file, the required scaling factor, translation distance and rotation information of the meshes is specified. With the existence of non-identical mesh node locations as shown in Fig. 2 along the boundaries of the individual cell zones of the computational domain, non-conformal interfaces are established between individual cell zones. These interfaces connect each cell zones by transferring fluxes from one mesh to another (ANSYS 2010). The first cell height from wall is kept at a distance of 0.001 m and grid spacing of 1.2 is maintained throughout the domain. The near-wall mesh was made fine enough to resolve the viscous sublayer ($y^+ < 5$) and the near-wall modelling was done through the enhanced wall treatment approach. The Three grid systems, namely 1002k (System1), 3202k (System 2) and 5110k (System 3), were created for the grid convergence study and airflow simulations were performed on each grid. To analyse the convergence of the three grid systems, the grid convergence index (GCI) concept was applied (Roache 1998; Wong et al. 2010). The root mean square of the relative error (e_{rms}) for the fluid flow mean velocities (u) detected at 100 points along a vertical line in the centre of the ward cubicle was used to determine the GCIs for the grid systems.

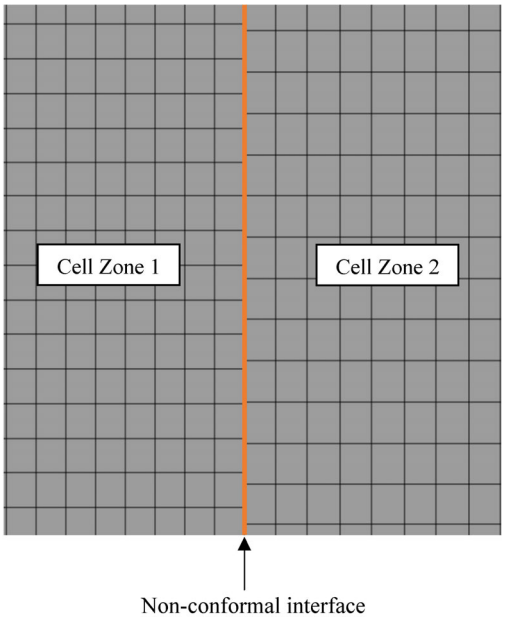

Fig. 2 Non-identical mesh nodes along the boundary of two cell zones

The GCI is calculated by:

$$\mathrm{GCI}(u) = F_s \frac{e_{rms}}{r^p - 1} \tag{4}$$

In the above equation, r is the grid refinement factor that is calculated as the ratio of the control volumes of fine and coarse grid systems, p is the order of the discretization method used, F_s is the safety factor and e_{rms} is determined by:

$$e_{rms} = \sqrt{\frac{\sum_{m=1}^{100} \left| \left(u_{m,coarse} - u_{m,fine} \right) / u_{m,fine} \right|^2}{100}} \tag{5}$$

$$r = \left(\frac{N_{fine}}{N_{coarse}} \right)^{1/3} \tag{6}$$

Using System 1 as a reference, the GCIs for Systems 2 and 3 were 3.11% and 3.40% respectively. As System 2 was adequate for studying the fluid flow characteristics, it was taken for further investigations by considering computational time as well as solution accuracy.

2.3.2 *Particle modelling*

The trajectories of individual particles were modelled using the Lagrangian framework and the modelling assumptions made are listed below (Tian et al. 2009; Zhao et al. 2004):

- The air-particle as well as particle-particle heat and mass transfers were neglected.
- A particle would not rebound when hitting a surface such as wall, ceiling and floor.
- Particle coagulation was neglected in the deposition process.
- All particles were modelled as spherical in shape.

The droplets exhaled through exhalation activities such as sneezing will shrink in size due to evaporation within a short period of time (< 0.1 s) (Xie et al. 2007). Their dried out residuals, the droplet nuclei, may be carrying pathogens (Wells 1955). In this study, a small percentage (< 10%) of the total virus laden droplets from a vigorous sneeze was assumed. It was proved that with such a small percentage, virus particles will not form clusters (Duguid 1946; Gralton et al. 2011). For simplicity's sake, droplet nuclei are referred to as particles in this article. The Lagrangian particle tracking calculates the discrete trajectories of individual particles in the fluid flow separately by solving the following particle

motion equation:

$$\frac{du_b}{dt} = \frac{18\mu}{\rho_b d_b^2}\frac{C_D Re}{24}(u_a - u_b) + \frac{g_a(\rho_b - \rho_a)}{\rho_b} + F_x \quad (7)$$

where u_a is the fluid velocity (m·s^{-1}), u_b is the particle velocity (m·s^{-1}), μ is the molecular viscosity of air (kg·m^{-1}·s^{-1}), ρ_a is the density of air (kg·m^{-3}), ρ_b is the particle density (kg·m^{-3}), d_b is the particle diameter (m), Re is the particle Reynolds number, C_D is the drag coefficient, g_a is the gravitational acceleration and F_x is the auxiliary forces acting on the particles. The particle Reynolds number is defined by,

$$Re = \frac{(u_a - u_b)d_b\rho_a}{\mu} \quad (8)$$

The drag coefficient C_D for the bioaerosol particles is defined by,

$$C_D = \frac{K_D}{Re_b}; \quad Re_b < 1 \quad (9)$$

The drag constant K_D for the bioaerosol particles as expressed in Eq. (9) is given by,

$$K_D = \frac{d_b^2}{2} \quad (10)$$

The above equations were solved in CFD simulations to determine the transport mechanisms of bioaerosol particles in a Lagrangian scheme. The validity of Eqs. (9) and (10) was established for a range of particles with equivalent bioaerosol diameters (d_b) from 0.69 μm to 6.9 μm and further examined for particles with d_b as low as 0.054 μm (Wong et al. 2015).

Apart from the drag force, forces that can influence particle motions include basset force, magnus force, virtual mass force, Brownian force and Saffman lift force. Although the magnitudes of these forces are greatly influenced by the fluid flow conditions and particle properties, a few of these forces are small enough to be neglected in some analyses (Zhao et al. 2004). Due to the particle size and non-isothermal flow conditions in this study, Brownian, thermophorectic and Saffman lift forces were taken into consideration for predicting the particle motion trajectories. The dispersion of particles as a consequence of turbulence in the flow field can be tracked through stochastic tracking methods. The discrete random walk (DRW) model, a popular approach that takes velocity fluctuations into account, was employed in this study (Lai et al. 2012). Further details for the CFD simulations are summarized in Table 1.

3 Results and discussions

The overall airflow distribution pattern based on ventilation strategies can have a great impact on the particle distribution within the space in a hospital ward. Figure 3 depicts the air velocity distribution and velocity vector plot across a horizontal plane located at y = 1.0 m for the base case, i.e. a typical ward cubicle without exhaust grilles. In Fig. 3(a), stagnant air with velocity less than 0.05 m·s^{-1} is observed near wall 2 and Fig. 3(b) depicts that the overall airflow pattern in the cubicle is directed towards the ward corridor. These results are consistent with those presented in our previous case study (Yu et al. 2017). Due to the existence of obstructions such as patients and beds, several eddies can be seen within the ward cubicle.

Figures 4 and 5 illustrate the temperature distribution as well as velocity vector plot across a vertical plane located at z = 1.625 m for an air change rate of 6 h^{-1} and 9 h^{-1} with EA = 50% respectively. As the thermal manikins cause thermal plumes, the effect of thermal plumes on the ward

Table 1 Parameters for the CFD simulations

Computational domain	7.5 m(L) × 6 m(W) × 2.7 m(H), RNG k-ε turbulence model with enhanced wall treatment
Total supply airflow rate	0.1240 kg·s^{-1} for ACH=3, 0.2480 kg·s^{-1} for ACH=6, 0.3720 kg·s^{-1} for ACH=9, 0.5374 kg·s^{-1} for ACH=13, 285 K (air temperature)
Inlet (0.6 m × 0.6 m) airflow rate	0.031 kg·s^{-1} for ACH=3, 0.0620 kg·s^{-1} for ACH=6, 0.093 kg·s^{-1} for ACH=9, 0.1343 kg·s^{-1} for ACH=13, 285 K (air temperature)
Diffuser (0.6 m × 0.6 m)	Four supply diffusers, 4-way spread pattern, air supplied at an angle of 15° from the ceiling, adiabatic
Corridor (6 m × 2.7 m)	Outflow with flow rate weighting, 295K (backflow temperature), adiabatic, escape boundary condition
Exhaust grille (0.5 m × 0.2 m)	Outflow with flow rate weighting, 295K (backflow temperature), adiabatic, escape boundary condition, exhaust air=0%/10%/50% of total supply air
Walls, ceiling, floor and beds	No-slip wall boundary, adiabatic, trap boundary condition
Patient	Six patients, no-slip wall boundary, 23.3 W·m^{-2} for each patient, trap boundary condition
Mouth of a patient (0.05 m × 0.05 m)	Single-shot release with an upward velocity v_b=50 m·s^{-1}, n_s=10,000 virus particles, bioaerosol density ρ_b= 1,100 kg·m^{-3}
Species (aerodynamic diameters)	MERS-CoV (0.167±0.012 μm)

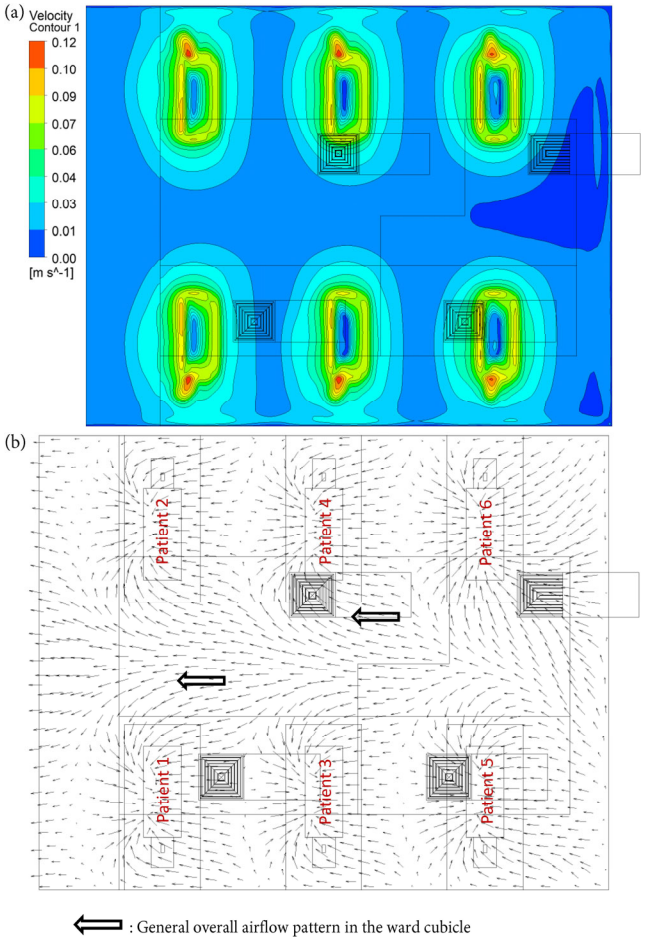

Fig. 3 Simulation results of the ward cubicle with no exhaust grilles at 6ACH: (a) air velocity distribution; (b) velocity vector plot

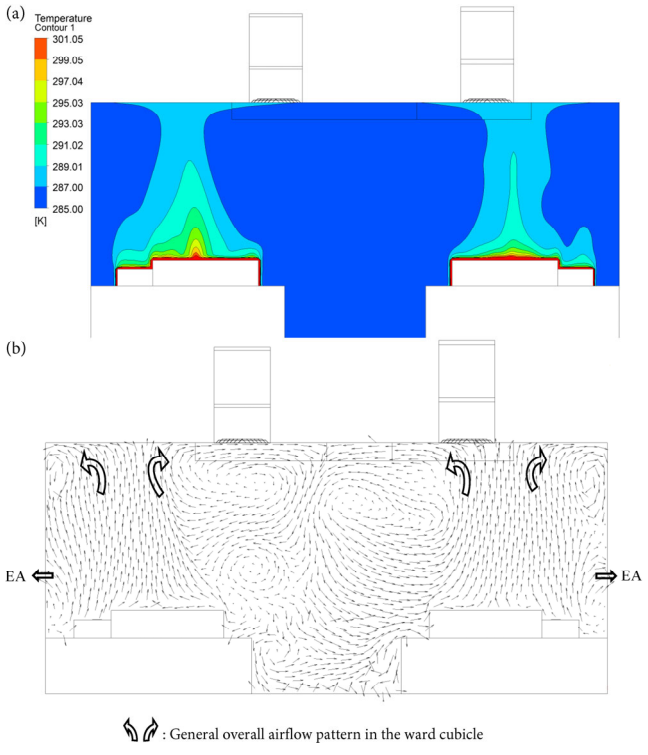

Fig. 4 Simulation results of ward cubicle with exhaust grilles at 6ACH and exhaust air (EA)=50%: (a) temperature distribution; (b) velocity vector plot

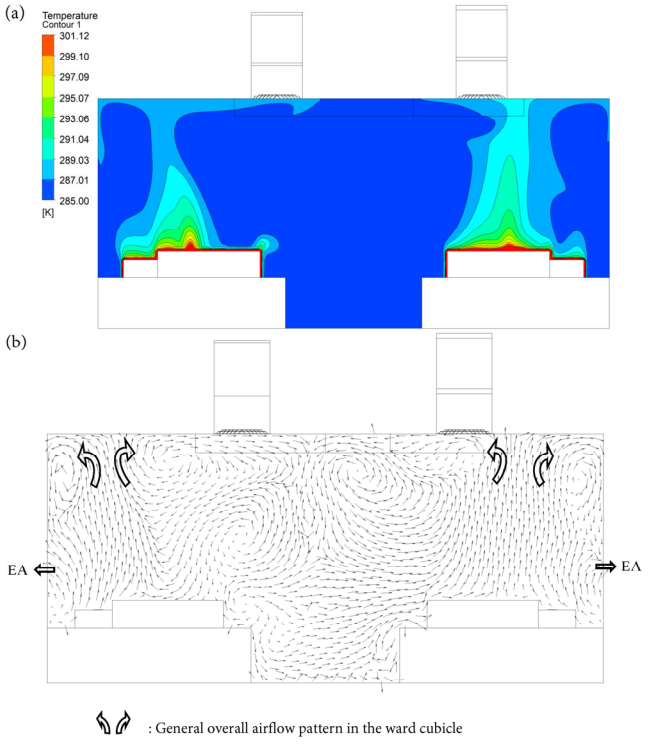

Fig. 5 Simulation results of ward cubicle with exhaust grilles at 9ACH and exhaust air (EA)=50%: (a) temperature distribution; (b) velocity vector plot

airflow pattern can be clearly seen from the vertical airflow distribution. There is an upward airflow (towards the ward ceiling) that returns to the floor level along the walls. Recirculation zones, which may occur when the cold supply air from the diffusers interacts with the upward airflow caused by the thermal plumes, are observed. These zones can enhance the mixing of air within the ward space. Moreover, the suction provided by the local exhaust grilles tends to alter the airflow pattern around a patient and thus can help to remove airborne contaminants in the immediate vicinity of the patient.

3.1 Cross infection within a ward cubicle

In the base case, almost half of the virus particles exhaled from a patient's mouth deposited onto the patient's body and bed. According to Fig. 6, there were considerable amounts of virus particles on different cubicle surfaces including walls, floor and ceiling. A maximum r_c ($\approx$ 0.26), resulted from the supine patients and their exhaled air velocities,

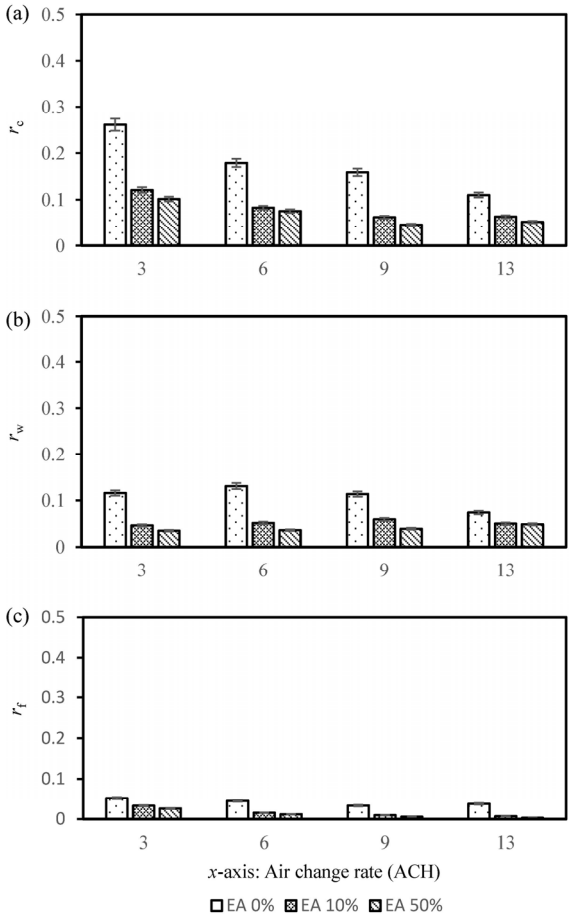

Fig. 6 ACH vs deposition ratio on: (a) ceiling; (b) walls; (c) floor

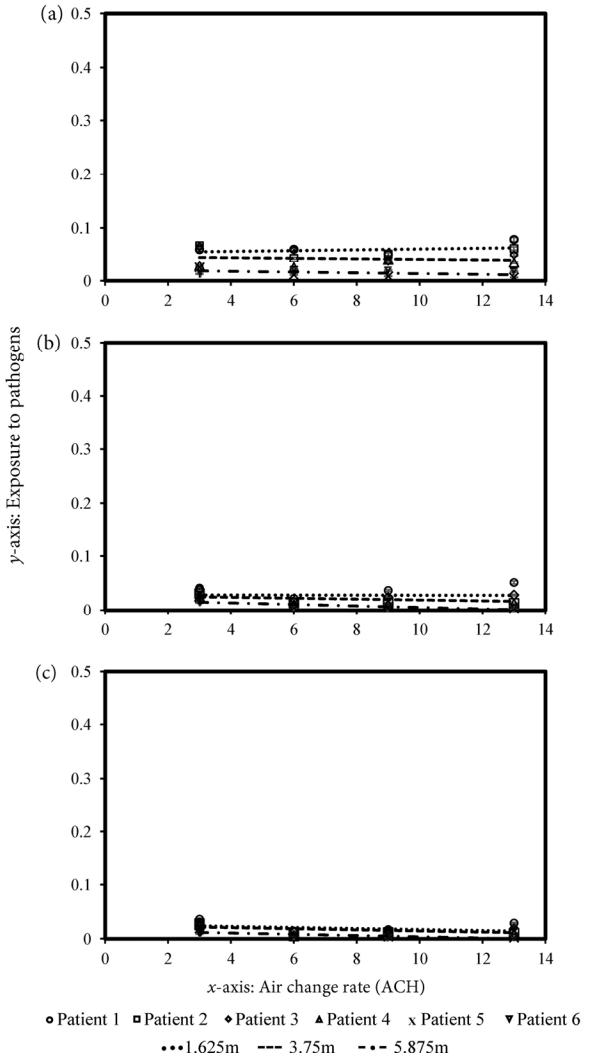

Fig. 7 ACH vs exposure to pathogens: (a) EA=0%; (b) EA=10%; (c) EA=50%

can be seen at 3 h^{-1} in Fig. 6(a). It can also be seen in the figure that r_c decreases as the air change rate increases (e.g. $r_c \approx 0.17$ at 6 h^{-1} (a 34% decrease) and $r_c \approx 0.11$ at 13 h^{-1} (a 57% decrease)). In fact, the air supplied through the diffusers has a higher momentum with an increased air change rate and it moves the particles away from the ceiling to other spaces within the cubicle. As depicted in Figs. 6(b) and (c), r_w and r_f were respectively greater than 0.07 and 0.03 in the base case for all air change rates.

As shown in Fig. 7(a), patients in beds located at 1.625 m away from the corridor (i.e. Patients 1 and 2) were most vulnerable to cross infection (with exposure risk (E) > 0.05) while those at 5.875 m away (i.e. Patients 5 and 6) were least (with E < 0.025). With an increase in air change rate, a significant reduction in infection risk was observed for patients located farther away from the corridor. This can be explained by the general airflow patterns as illustrated in Fig. 3. On average, the infection risk level of Patients 5 and 6 was only half of that of Patients 1 and 2 for all air change rates.

Figures 4 and 5 demonstrate that the local exhaust grilles not only facilitated the removal of a portion of exhaled virus particles but also tended to increase the particle deposition in the source patient's body and thereby reduced the residual viral load present in the air. As exhibited in Fig. 6(a), the recorded values of r_c at 3 h^{-1} were approximately 0.12 and 0.10 for EA = 10% and EA = 50% (i.e. decreases of 53% and 61%; comparing with the base case) respectively. For all other cases shown in the figure, similarly, r_c decreased as the air change rate increased. According to Figs. 6(b) and (c), wall and floor deposition ratios were also significantly reduced with EA = 10% and 50% (r_w < 0.05 and r_f < 0.03).

However, deposition of particles was observed in all scenarios. As the deposition is random in nature and often happens irrespective of the ventilation system design, it highlights the importance of regular and proper ward housekeeping. Furthermore, the randomness associated with particle deposition rates (r_w, r_c, and r_f) under different air change rate conditions can be attributed to the asymmetric airflow distribution patterns and locations of the infected patients.

Figures 7(b) and (c) indicate that the installation of exhaust grilles in close proximity to each patient can help prevent particle migration from an infected patient to different locations in the ward and significantly reduce individual patient exposures ($E < 0.05$). The results show that the location of an infected patient, exhaust airflow rates and air change rates within the cubicle work together influencing the mechanism of viral spread.

3.2 Infection from a ward cubicle to the corridor

The pathogen spatial distribution is dependent on the ward layout, ventilation strategy and location of the source patient. It can be observed in Fig. 8(a) that exhausted ratio r_e increases with air change rate in the base case. The maximum r_e was recorded for Patients 1 and 2. From $r_e < 0.05$ at 3 h^{-1} to $r_e > 0.25$ at 13 h^{-1}, an abrupt increase in risk (80%) was noted for these patients. At higher air change rates, specifically at 13 h^{-1}, the number of particles reaching the corridor due to the exhalation activities of Patients 5 and 6 located at the rear end of the ward (i.e. 5.875 m away from corridor) was quite high ($0.05 < r_e < 0.1$). This suggests that the use of a high air change rate such as 13 h^{-1} can put the users of the corridor and its connected amenities at high risk of exposure to pathogens and facilitate infectious disease outbreaks in the whole healthcare facility.

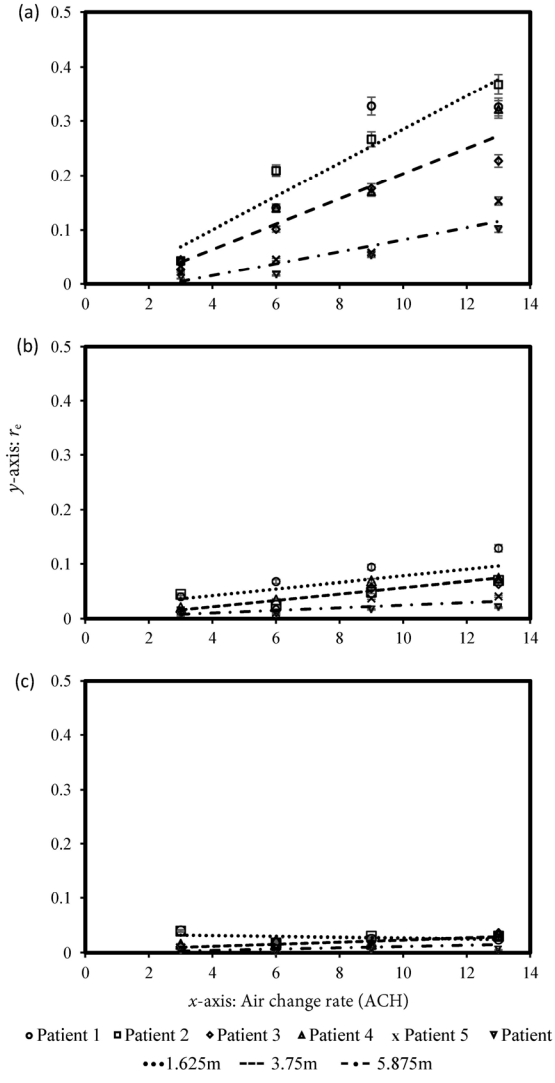

Fig. 8 ACH vs exhausted ratio: (a) EA=0%; (b) EA=10%; (c) EA=50%

As shown in Figs. 8(b) and (c), the installation of exhaust grilles considerably reduced the risk of infection transmission. The exhaust grilles lowered the r_e values of Patients 1 and 2 at 13 h^{-1} to 0.15 with EA = 10% (i.e. a decrease of 40%; comparing with the base case) and < 0.03 with EA = 50% (i.e. a decrease of 88%; comparing with the base case). Specifically, the supine patients at the rear end of the ward cubicle (i.e. Patients 5 and 6) contributed the least to the spread of infection to the corridor ($r_e < 0.006$). As the local exhaust airflow rate proved effective in reducing the risk of infection transmission, both the location and airflow rate of an exhaust grille are crucial factors for designing infection control strategies.

4 Conclusion

This study investigated the transport mechanism and deposition patterns of MERS-CoV within an air-conditioned general inpatient ward cubicle. It demonstrated that both air change and exhaust airflow rates have significant effects on not only the airflow but also the particle distribution within a mechanically ventilated space. Moreover, the location of an infected patient within the ward cubicle is crucial in determining the extent of infection risk to other ward occupants. Hence, it is recommended to provide exhaust grilles in close proximity to a patient, preferably above each patient's bed. To achieve infection prevention and control, high exhaust airflow rate is also suggested. Regardless of the ventilation design, all patients and any surfaces within a ward cubicle should be regularly and thoroughly cleaned and disinfected to remove microbial contamination. Installation of UVGI lamps in the ward space is recommended to further enhance the risk mitigation strategies. The outcome of this study can serve as a source of reference for hospital management to better ventilation design strategies for mitigating the risk of infection.

Acknowledgements

This work was partially supported by the Research Grants Council of HKSAR and The Hong Kong Polytechnic University (Project No. 15208817E).

References

ANSYS (2010). Ansys Fluent 13.0 Documentation. Lebanon, NH, USA: Ansys Inc.

ASHRAE (2013a). ASHRAE Standard. Ventilation for Health Care Facilities. Atlanta, GA, USA: American Society of Heating, Refrigerating and Air-Conditioning Engineers.

ASHRAE (2013b). ASHRAE Fundamentals SI Handbook. Atlanta, GA, USA: American Society of Heating, Refrigerating and Air-Conditioning Engineers.

Beggs CB, Kerr KG, Noakes CJ, Hathway EA, Sleigh PA (2008). The ventilation of multiple-bed hospital wards: Review and analysis. *American Journal of Infection Control*, 36: 250–259.

Blocken B (2018). LES over RANS in building simulation for outdoor and indoor applications: a foregone conclusion? *Building Simulation*, 11: 821–870.

Bolashikov Z, Melikov A, Kierat W, Popiołek Z, Brand M (2012). Exposure of health care workers and occupants to coughed airborne pathogens in a double-bed hospital patient room with overhead mixing ventilation. *HVAC & R Research*, 18: 602–615.

Chao CYH, Wan MP, Sze To GN (2008). Transport and removal of expiratory droplets in hospital ward environment. *Aerosol Science and Technology*, 42: 377–394.

Chaudhury H, Mahmood A, Valente M (2005). Advantages and disadvantages of single-versus multiple-occupancy rooms in acute care environments: A review and analysis of the literature. *Environment and Behavior*, 37: 760–786.

Chen Q (1995). Comparison of different k-ε models for indoor air flow computations. *Numerical Heat Transfer, Part B: Fundamentals,* 28: 353–369.

Chen C, Zhao B, Yang X, Li Y (2011). Role of two-way airflow owing to temperature difference in severe acute respiratory syndrome transmission: Revisiting the largest nosocomial severe acute respiratory syndrome outbreak in Hong Kong. *Journal of the Royal Society Interface*, 8: 699–710.

Duguid JP (1946). The size and the duration of air-carriage of respiratory droplets and droplet-nuclei. *Journal of Hygiene,* 44: 471–479.

Gao NP, Niu JL (2005). CFD study of the thermal environment around a human body: A review. *Indoor and Built Environment*, 14: 5–16.

Ghia U, Konangi S, Kishore A, Gressel M, Mead K, Earnest G (2012). Assessment of health-care worker exposure to pandemic flu in hospital rooms. *ASHRAE Transactions*, 118(1): 442–449.

Giannini MA, Nance D, McCullers JA (2009). Are toilet seats a vector for transmission of methicillin-resistant Staphylococcus aureus? *American Journal of Infection Control*, 37: 505–506.

Gralton J, Tovey E, McLaws ML, Rawlinson WD (2011). The role of particle size in aerosolised pathogen transmission: A review. *Journal of Infection*, 62: 1–13.

Hang J, Li Y, Jin R (2014). The influence of human walking on the flow and airborne transmission in a six-bed isolation room: Tracer gas simulation. *Building and Environment*, 77: 119–134.

Humphreys H (2006). Overcrowding, understaffing and infection in hospitals. *Irish Medical Journal*, 99: 102.[PubMed]

Kim SH, Chang SY, Sung M, Park JH, Bin Kim H, Lee H, Choi JP, Choi WS, Min JY (2016). Extensive viable middle east respiratory syndrome (MERS) coronavirus contamination in air and surrounding environment in MERS isolation wards. *Clinical Infectious Diseases*, 63: 363–369.

Lai ACK, Wong LT, Mui KW, Chan WY, Yu HC (2012). An experimental study of bioaerosol (1–10 μm) deposition in a ventilated chamber. *Building and Environment*, 56: 118–126.

Li Y, Huang X, Yu ITS, Wong TW, Qian H (2005). Role of air distribution in SARS transmission during the largest nosocomial outbreak in Hong Kong. *Indoor Air*, 15: 83–95.

Li Y, Leung GM, Tang JW, Yang X, Chao CYH, Lin JZ, Lu JW, Nielsen PV, Niu J, Qian H, Sleigh AC, Su HJJ, Sundell J, Wong TW, Yuen PL (2007). Role of ventilation in airborne transmission of infectious agents in the built environment—A multidisciplinary systematic review. *Indoor Air*, 17: 2–18.

Li Y, Tang J, Noakes C, Hodgson MJ (2015). Engineering control of respiratory infection and low-energy design of healthcare facilities. *Science and Technology for the Built Environment*, 21: 25–34.

Licina D, Melikov A, Pantelic J, Sekhar C, Tham KW (2015). Human convection flow in spaces with and without ventilation: Personal exposure to floor-released particles and cough-released droplets. *Indoor Air*, 25: 672–682.

Memarzadeh F, Xu W (2012). Role of air changes per hour (ACH) in possible transmission of airborne infections. *Building Simulation*, 5: 15–28.

Nicas M, Hubbard AE, Jones RM, Reingold AL (2004). The infectious dose of variola (smallpox) virus. *Applied Biosafety*, 9: 118–127.

Nielsen PV (2015). Fifty years of CFD for room air distribution. *Building and Environment*, 91: 78–90.

Oh MD, Park WB, Park SW, Choe PG, Bang JH, Song KH, Kim ES, Kim HB, Kim NJ (2018). Middle East respiratory syndrome: What we learned from the 2015 outbreak in the Republic of Korea. *Korean Journal of Internal Medicine,* 33: 233-246.

Pantelic J, Tham KW (2013). Adequacy of air change rate as the sole indicator of an air distribution system's effectiveness to mitigate airborne infectious disease transmission caused by a cough release in the room with overhead mixing ventilation: A case study. *HVAC&R Research*, 19: 947–961.

Qian H, Li Y (2010). Removal of exhaled particles by ventilation and deposition in a multibed airborne infection isolation room. *Indoor Air*, 20: 284–297.

Roache PJ (1998). Verification of codes and calculations. *AIAA Journal*, 36: 696–702.

Roy CJ, Milton DK (2004). Airborne transmission of communicable infection—the elusive pathway. *New England Journal of Medicine*, 350: 1710–1712.

Shen C, Gao N, Wang T (2013). CFD study on the transmission of indoor pollutants under personalized ventilation. *Building and Environment*, 63: 69–78.

Tang JW, Wilson P, Shetty N, Noakes CJ (2015). Aerosol-transmitted infections—A new consideration for public health and infection control teams. *Current Treatment Options in Infectious Diseases*, 7: 176–201.

Tian L, Lin Z, Wang Q, Liu J (2009). Numerical investigation of indoor aerosol particle dispersion under stratum ventilation and under displacement ventilation. *Indoor and Built Environment*, 18: 360–375.

Van Doremalen N, Bushmaker T, Munster VJE (2013). Stability of Middle East respiratory syndrome coronavirus (MERS-CoV) under different environmental conditions. *Euro Surveillance*, 18: 20590.

Wan MP, Chao CYH, Ng YD, Sze To GN, Yu WC (2007). Dispersion of expiratory droplets in a general hospital ward with ceiling mixing type mechanical ventilation system. *Aerosol Science and Technology*, 41: 244–258.

Wells WF (1955). Airborne Contagion and Air Hygiene. An Ecological Study of Droplet Infections. Cambridge, USA: Harvard University Press.

Wong LT, Chan WY, Mui KW, Lai ACK (2010). An experimental and numerical study on deposition of bioaerosols in a scaled chamber. *Aerosol Science and Technology*, 44: 117–128.

Wong LT, Yu HC, Mui KW, Chan WY (2015). Drag constants for common indoor bioaerosols. *Indoor and Built Environment*, 24: 401–413.

Xiao S, Li Y, Sung M, Wei J, Yang Z (2018). A study of the probable transmission routes of MERS-CoV during the first hospital outbreak in the Republic of Korea. *Indoor Air*, 28: 51–63.

Xie X, Li Y, Chwang ATY, Ho PL, Seto WH (2007). How far droplets can move in indoor environments—revisiting the Wells evaporation-falling curve. *Indoor Air,* 17: 211-225.

Yu HC, Mui KW, Wong LT, Chu HS (2017). Ventilation of general hospital wards for mitigating infection risks of three kinds of viruses including Middle East respiratory syndrome coronavirus. *Indoor and Built Environment*, 26: 514–527.

Zeytounian RK (2003). Joseph Boussinesq and his approximation: A contemporary view. *Comptes Rendus Mécanique*, 331: 575–586.

Zhang Z, Chen Q (2006). Experimental measurements and numerical simulations of particle transport and distribution in ventilated rooms. *Atmospheric Environment*, 40: 3396–3408.

Zhang Z, Chen Q (2007). Comparison of the Eulerian and Lagrangian methods for predicting particle transport in enclosed spaces. *Atmospheric Environment*, 41: 5236–5248.

Zhang Z, Zhang W, Zhai ZJ, Chen QY (2007). Evaluation of various turbulence models in predicting airflow and turbulence in enclosed environments by CFD: part 2—comparison with experimental data from literature. *HVAC&R Research*, 13: 871–886.

Zhao B, Zhang Y, Li X, Yang X, Huang D (2004). Comparison of indoor aerosol particle concentration and deposition in different ventilated rooms by numerical method. *Building and Environment*, 39: 1–8.

Zumla A, Hui DS, Perlman S (2015). Middle East respiratory syndrome. *The Lancet*, 386: 995–1007.